Chemical Science

Accepted Manuscript

This article can be cited before page numbers have been issued, to do this please use: C. Sabrià, T. Pèlachs, I. Imaz, D. Maspoch, F. Feixas and X. Ribas, *Chem. Sci.*, 2026, DOI: 10.1039/D6SC02321E.

ROYAL SOCIETY OF CHEMISTRY

rsc.li/chemical-science

View Article Online
DOI: 10.1039/D6SC02321E

ARTICLE

Supramolecular Purification of Mono-Adamantane Mixtures via Stabilized Three-Shell Matryoshka Assemblies

Received 00th January 20xx,
Accepted 00th January 20xx

DOI: 10.1039/x0xx00000x

Clara Sabrià,[a] Tània Pèlachs,[a] Inhar Imaz,[b] Daniel Maspoch,[b,c] Ferran Feixas,*[a] and Xavi Ribas*[a]

The adamantane (Ad) core is widely used in pharmaceuticals, where it is regarded as a lipophilic "bullet" that enhances the bioactivity of Ad-bearing drugs. Despite its prevalence, little is known about its precise recognition modes within confined enzymatic active sites, and effective chromatographic strategies for the purification of mixtures of Ad derivatives remain limited. Herein, we report the supramolecular purification of mono-adamantane mixtures through the development of three-shell supramolecular Matryoshka assemblies, featuring an adamantane–cycloparaphenylene (CPP) host–guest adduct encapsulated within a tetragonal prismatic nanocage. This three-shell architecture operates via an all-in-one strategy: encapsulation is inefficient for either [8]CPP or diamondoids alone and occurs efficiently only when all three components are present simultaneously. A straightforward, solid-state filtration–redissolution protocol enables the purification of diamondoid mixtures with enhanced selectivity for amine-bearing adamantane derivatives. This approach demonstrates a high degree of supramolecular selectivity in complex diamondoid mixtures, potentially exceeding that of conventional chromatographic techniques.

Introduction

1-Adamantane monoderivatives -including amantadine, rimantadine, Ad-alkylamides, Ad-halides, Ad-COOH, and Ad-alcohols, among others- have been widely employed as therapeutic agents for numerous diseases. In addition, they serve as versatile building blocks for introducing the $C_{10}H_{15}$ adamantyl moiety into hundreds of pharmaceutical compounds via esterification, amidation, coupling, and related transformations. Since the discovery of the antiviral activity of amantadine (1-Ad-NH_2) in 1964,[1] numerous antivirals and other pharmaceuticals incorporating this adamantyl unit have been identified. Notably, the pseudo-spherical three-dimensional structure of adamantane imparts critical lipophilicity to these compounds, enhancing their therapeutic efficacy and establishing adamantane as one of the most successful hydrocarbon motifs for improving or conferring pharmacological activity.[2, 3] Resistance to amantadine as an antiviral agent has shifted its therapeutic application, and it is now used to treat dyskinesia associated with Parkinson's disease (Figure 1a).[4] Rimantadine, which contains an alkylamine group, exhibits very low hepatotoxicity and is recommended as a prophylactic agent for the prevention of Influenza A in high-risk settings such as nursing homes (Figure 1a).[5] At the same time, subtle stereoelectronic or conformational changes can have a pronounced impact on antiviral efficacy. This effect is illustrated by comparisons between 2-rimantadine and 2-amantadine (substitution at a secondary carbon) and their corresponding 1-adamantyl analogues (substitution at a tertiary carbon).

On the other hand, higher diamondoid derivatives such as diamantane and triamantane represent minimal molecular fragments of the diamond lattice and have been explored as diamond precursors (Figure 1a).[6] In addition, a range of advanced applications of diamondoid-containing materials has been developed, including electron emitters and catalytic sensors, owing to their intrinsic properties such as negative electron affinity, substantial steric bulk, and electron-donating ability.[7] Diamondoid molecules have also demonstrated significant potential in micro- and nanoelectronic applications due to their quantum confinement effects and tunable band gaps.[8]

Overall, regardless of their target application, the separation and purification of diamondoid-based mixtures remain chromatographically challenging.[9] Selective purification via supramolecular encapsulation is unprecedented and, if achieved, would represent a disruptive strategy for the direct isolation of specific derivatives obtained from a single synthetic sequence. In this context, Wang and co-workers reported unsuccessful attempts to supramolecularly differentiate adamantane monoderivatives (Ad, Ad–CH2OH, and Ad–COOH) using Ag- or Hg-based cages; their study instead focused on the dual-controlled release of each guest (Figure 1b).[10] Conversely, Han and co-workers reported supramolecular porous materials featuring a uniquely partitioned cavity that functions as a multifunctional extractant for the separation of brominated

[a] Institut de Química Computacional i Catàlisi (IQCC) and Departament de Química, Universitat de Girona, Campus Montilivi, 17003 Girona, Catalonia (Spain). E-mail: ferran.feixas@udg.edu, xavi.ribas@udg.edu
[b] Catalan Institute of Nanoscience and Nanotechnology (ICN2), CSIC and The Barcelona Institute of Science and Technology, Campus UAB, 08193, Bellaterra, Catalonia (Spain)
[c] ICREA, Pg. Lluís Companys 23, 08010 Barcelona (Spain)

View Article Online
DOI: 10.1039/D5SC02721F

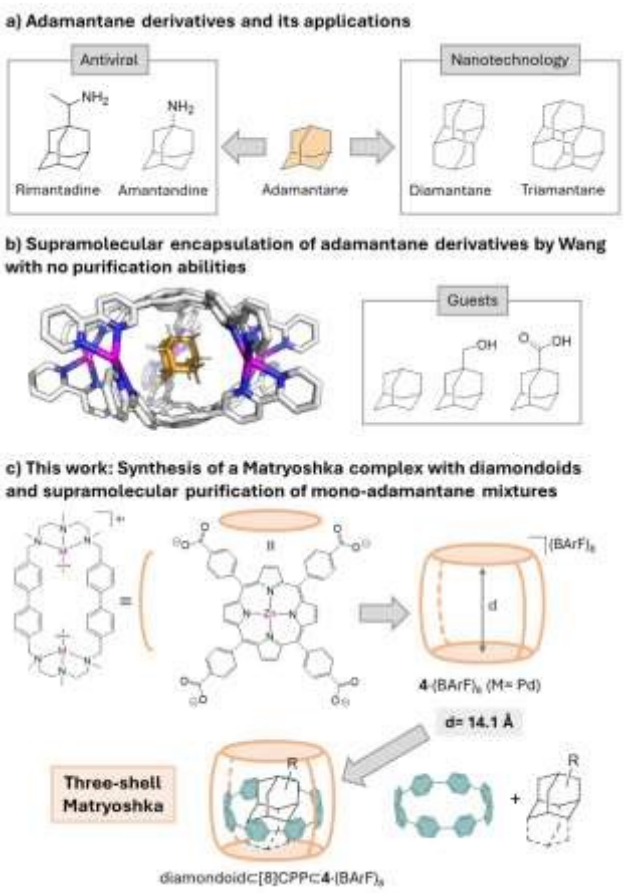

Figure 1. a) Structure of adamantane and some amine-substituted adamantanes as antiviral drugs in medicine (antiviral/anti-Parkinson) (on the left) and higher diamondoids used in nanotechnology (on the right). b) Encapsulation of mono-adamantane derivatives into a supramolecular Ag-based cage.[10] c) (This work) Synthesis of a three-shell Matryoshka complex featuring a diamondoid⊂[8]CPP host-guest adduct inside a tetragonal prismatic supramolecular cage.

adamantanes and small polycyclic aromatic hydrocarbons (PAHs).[11]

Inspired by the efficient and aesthetic encapsulation of spherical diamondoids (e.g. adamantane, diamantane, and others) in carbon nanotubes[12, 13] and metallocages,[14] herein we present the exquisite supramolecular purification of mono-adamantane mixtures by developing three-shell supramolecular Matryoshkas. These assemblies feature an adamantane-cycloparaphenylene (CPP)[15, 16] host-guest adduct encapsulated in a tetragonal prismatic nanocage **4**·$(BArF)_8$ (Figure 1c). CPPs are fully conjugated macrocyclic hydrocarbons that have promising applications in supramolecular systems.[17, 18] They are known to bind many fullerenes, stabilizing them via π-π interactions[19, 20] and enabling the synthesis of C_{60}/CPP-based [2]catenanes.[21, 22] More recently, they have been shown to encapsulate other molecules via C-H···π interactions, such as metallocenes[23] or polycyclic aromatic hydrocarbons (PAHs).[24] Our group has previously reported size-tunable tetragonal prismatic cages formed by two Zn-TCPP (5,10,15,20-tetrakis (4-carboxyphenyl)-porphyrin Zn(II)) units acting as the apical "caps", and four Pd(II) macrocyclic complexes forming the walls.[25, 26] The cage size can be tuned by varying the Zn-Zn distance through the use of different macrocyclic clips. As well, a three-shell Matryoshka complex has been previously reported by our group, consisting of a C_{60}⊂[10]CPP complex encapsulated inside the **6**·$(BArF)_8$ cage, with a Zn-Zn distance of 16.8 Å.[27] In the present work, a smaller nanocage **4**·$(BArF)_8$ with a Zn-Zn distance of 14.1 Å is used, which is known to exhibit high affinity towards fullerenes[28, 29] and pyridine-based catalysts.[30] The stability of the three-shell complexes reported herein arises from apical-Zn-TCPP anchoring of the mono-adamantane moiety and the stabilization of the CPP ring within the cavity. Notably, efficient complex formation occurs only when all three components are present simultaneously, resulting in a marked enhancement in stability. Nevertheless, subtle structural differences among the adamantane derivatives translate into clear trends in encapsulation affinity, enabling a straightforward solid–liquid supramolecular filtration–purification process.

Results and discussion

With the aim of encapsulating diamondoids in a minimalistic form of a carbon nanotube, simple cycloparaphenylene (CPP) nanorings were selected as hosts. The diameter of CPPs depends on the number of phenyl rings they contain (9.8 Å for [7]CPP, 11 Å for [8]CPP, 12 Å for [9]CPP, and 13.7 Å for [10]CPP). Accordingly, molecular dynamics (MD) simulations were used to predict which CPP provides the most suitable diameter to encapsulate diamondoids. Adamantane (**i**), the smallest diamondoid, has an approximate size of 4.3 Å, whereas diamantane (**e**) has the same size on the shortest axis but extends to 6.9 Å along its longest axis (Figure S90a). These two diamondoids were selected as guest models for simulations with [n]CPP nanorings (n = 7, 8, and 9).

Spontaneous binding MD simulations were performed in acetonitrile (MeCN), starting with the unbound diamondoid placed ~15 Å from the center of the nanoring, in order to assess the encapsulation and guest stability. Among all the nanorings studied, only [8]CPP (eight phenyl rings, diameter ≈ 11 Å; Figure S90) transiently accommodated both adamantane **i** and diamantane **e**. Based on this result, experimental encapsulation was carried out using various adamantane derivatives by mixing equimolar amounts of guest and host ([8]CPP) in dichloromethane (DCM). ^{1}H-NMR analysis revealed small chemical shifts for both [8]CPP and guest (Figures S1–S14), corresponding to very low association constants ($<0.5 \times 10^2$ M^{-1}) (Table S1), in line with the transient binding observed in the MD simulations. These results clearly indicate that [8]CPP alone is insufficient to stabilize the diamondoid⊂[8]CPP assembly.

To further stabilize the diamondoid⊂[8]CPP complex through additional confinement, its encapsulation within the cavity of the tetragonal prismatic nanocage **4**·$(BArF)_8$ was studied experimentally. First, the encapsulation of [8]CPP was carried out by adding two equivalents of [8]CPP in DCM to a solution of the cage in MeCN, followed by stirring at room temperature

View Article Online
DOI: 10.1039/D6SC02321E

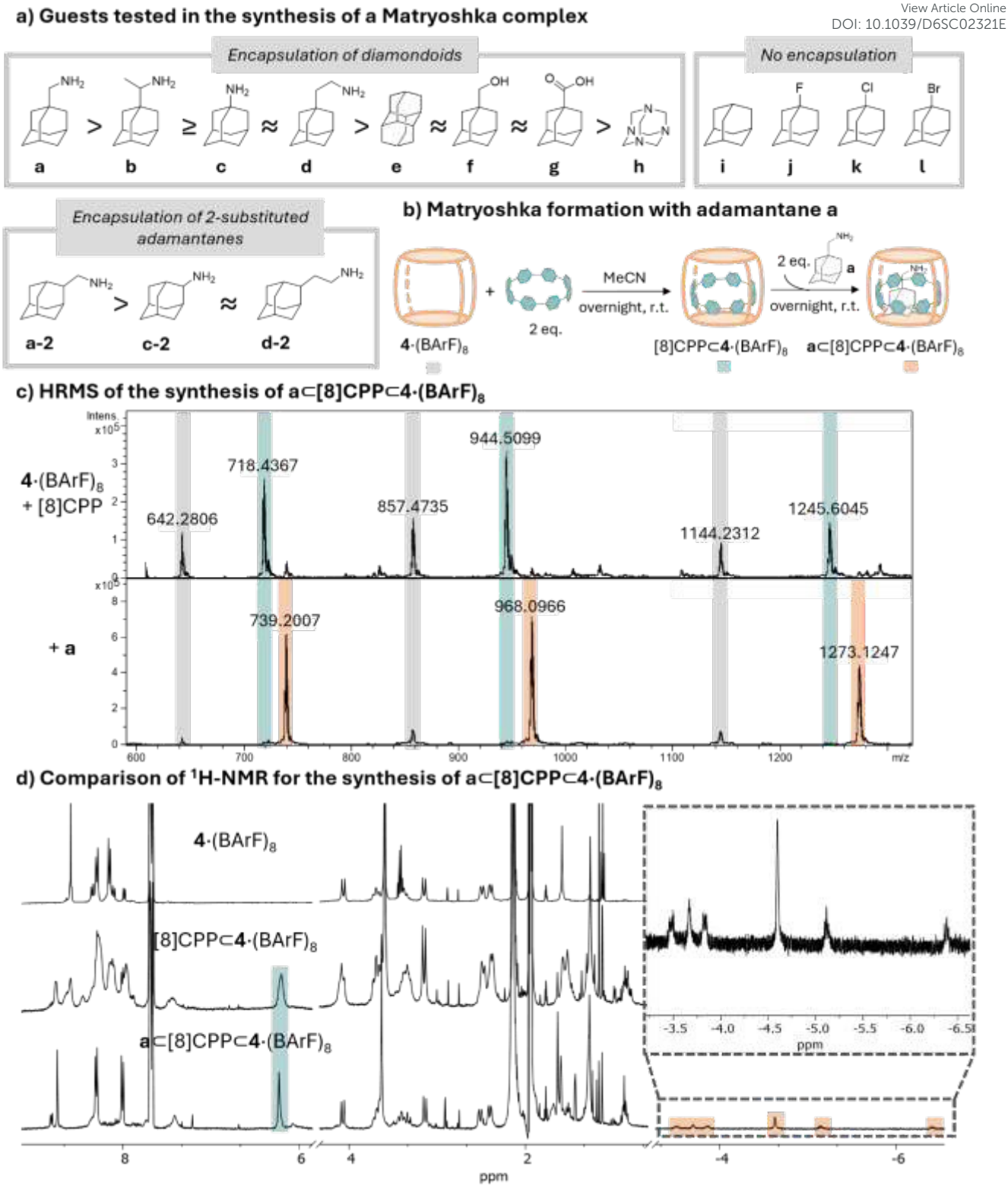

Figure 2. a) Structure of the guest tested for encapsulation, showing the ones that give the formation of a diamondoid⊂[8]CPP⊂**4**·$(BArF)_8$ Matryoshka complex on the top left (**a-h**), those 2-substituted that show encapsulation on the bottom (**a-2**, **c-2**, and **d-2**) and those that do not on the top right (**i-l**); guests that form the Matryoshka complex are in order of affinity. b) Synthesis of a Matryoshka complex using cage **4**·$(BArF)_8$ with [8]CPP and the adamantane derivative **a** containing an amine substituent. c) HRMS spectra of the encapsulation of [8]CPP (top) and the subsequent encapsulation of guest **a** (bottom) to give the formation of the Matryoshka complex **a**⊂[8]CPP⊂**4**·$(BArF)_8$. d) Stacked ^{1}H-NMR spectra (CD_3CN) for the empty cage (top), [8]CPP⊂**4**·$(BArF)_8$ (middle), and **a**⊂[8]CPP⊂**4**·$(BArF)_8$ (bottom). The peak of the encapsulated [8]CPP is marked in blue, and peaks of the encapsulated adamantane **a** (at negative chemical shifts) are marked in orange and zoomed.

View Article Online
DOI: 10.1039/D6SC02321E

ARTICLE

overnight. Successful encapsulation was confirmed by high-resolution mass spectrometry (HRMS) (Figure 2c and S15) and ^{1}H-NMR spectroscopy, which showed broadening of the cage signals and the appearance of a new signal at 6.21 ppm corresponding to encapsulated [8]CPP (Figure 2d and Figures S16–S17).

The formation of a Matryoshka-like complex was then investigated by adding adamantane derivatives (Figure 2a). In a typical procedure, two equivalents of the adamantane guest in DCM were added to a preformed solution of [8]CPP⊂**4**·$(BArF)_8$ in MeCN. The mixture was stirred at room temperature overnight and analyzed by HRMS and ^{1}H-NMR. Initial tests with unsubstituted adamantane were unsuccessful, and only signals corresponding to [8]CPP encapsulation were observed in the HRMS spectra. We hypothesized that the introduction of an amine group to the adamantane core could enable stable encapsulation via coordination of the N atom to the Zn ion of the porphyrin unit. Accordingly, adamantanes bearing amine groups at position 1 (**a-d**) were tested, confirming their encapsulation by HRMS for all four guests (Figures 2c, S18, S25, S28, and S31). The ^{1}H-NMR spectra revealed a new set of signals for the cage, consistent with Matryoshka complex formation, along with a new set of peaks in the negative region corresponding to the adamantane guests (Figures 2d, S19, S26, S29, S32). The upfield shifts of the amine-substituted adamantanes indicate confinement within the supramolecular cage cavity. These results demonstrate that amine-substituted adamantanes with chains of varying lengths (–NH_2 for **c**, –CH_2NH_2 for **a**, and –$CH_2CH_2NH_2$ for **d**) can form the three-shell Matryoshka complex. Notably, even the presence of a methyl group at the α-position to the amine, as in rimantadine **b**, does not disrupt Zn···N coordination, and the Matryoshka complex formation is still observed. The adamantane derivative **h**, containing four amine groups replacing the tertiary carbons of the adamantane core, also forms the Matryoshka complex (Figures S47–S49), as evidenced by HRMS; however, peaks corresponding to the sole encapsulation of [8]CPP are similarly prominent, suggesting a smaller association constant than for **a-d**, and comparable to that of [8]CPP alone. Interestingly, some diamondoids lacking amine groups were also weakly encapsulated, including diamantane **e** (Figures S38–S40), 1-adamantanemethanol (**f**) (Figures S41–S43), and 1-adamantanecarboxylic acid (**g**) (Figures S44–S46). In contrast, adamantanes containing halogens (–F for **j**, –Cl for **k**, and –Br for **l**) showed no evidence of encapsulation by either HRMS or ^{1}H-NMR (Figures S59–S60).

The 2-adamantane analogues (substitution at the tertiary carbon) of the amine-substituted guests **a**, **c**, and **d** were also examined (**a-2**, **c-2**, and **d-2**). Encapsulation was confirmed for all by HRMS and ^{1}H-NMR (Figures S50–S58), with no noticeable differences compared to their 1-substituted counterparts.

Finally, encapsulation experiments performed for all tested diamondoids in the absence of [8]CPP and using only the nanocage **4**·$(BArF)_8$, showed no evidence of host–guest assemblies by HRMS or ^{1}H-NMR (Figures S61–S64), with only signals corresponding to empty cage being detected.

Competition experiments

We hypothesized that fine-tuning the substitution of the adamantane core would significantly influence the affinity of each mono-adamantane guest, arising from a dual stabilization mechanism: encapsulation within the [8]CPP nanoring and anchoring to the Zn–TCPP moiety of the cage. To test this hypothesis, competition experiments were conducted among the different adamantane derivatives and monitored by HRMS and ^{1}H-NMR, allowing us to establish an affinity trend for derivatives **a-h** (Figure 2a). When mixtures of amine-1-substituted adamantanes and diamantane (**a-c** and **e**) were examined in the presence of [8]CPP⊂**4**·$(BArF)_8$, only guest **a** was observed to be encapsulated by HRMS (Figure S65). In contrast, when **b**, **c**, and **e** were combined, HRMS showed encapsulation of **b** and **c** in a 2:1 ratio, with no inclusion of **e** (Figure S67). Similarly, competition between amine-containing adamantanes **c** and **d** yielded the Matryoshka complex in a 1:1 ratio (Figure S68). These results indicate that cage **4**·$(BArF)_8$ exhibits higher affinity for amine-bearing 1-substituted adamantanes driven by Zn···N coordination, whereas diamantane **e**, lacking an anchoring group, shows negligible binding in the presence of amine-1-substituted adamantanes. The presence of a CH_2 spacer between the adamantane core and the amine in guest **a**, compared to amantadine (**c**), favored the Zn···N axial-metal ligand coordination while stabilizing the adamantane in the nanoring and maintaining [8]CPP at a non-repulsive distance from the porphyrin. In the case of rimantadine (**b**), which features a methyl group next to the amine substituent while retaining the same chain length, the affinity is reduced compared to **a**, likely due to the clashing of the methyl with the porphyrin and the nanoring (see below). On the other hand, when the amine is directly attached to the adamantane core (**c**) or separated by two CH_2 units (**d**), the affinity is further diminished. Finally, bare diamantane (**e**), which cannot engage in Zn···N coordination, also displays low affinity. Interestingly, when the smallest nitrogen-containing adamantane **h** was mixed with diamantane **e**, HRMS revealed predominant encapsulation of **e** along with minor peaks corresponding to **h** (Figure S72). The steric hindrance between the porphyrin can rationalize this behavior and [8]CPP, imposed when the nitrogen atom is directly attached to the adamantane core,

View Article Online
DOI: 10.1039/D5SC03215F

weakening the Zn···N interaction with the porphyrin. Finally, when diamantane **e** was combined with adamantanes **f** and **g**, the Matryoshka complexes were formed in comparable amounts for all three guests (Figure S71), indicating nearly equivalent affinities. These results suggest that guests **f** and **g** may engage in weak attractive interactions with the Zn–TCPP unit, while the elongated size of **e** contributes to its stabilization within the Matryoshka complex.

The amine-2-substituted adamantanes **a-2**, **c-2**, and **d-2** exhibit the same affinity trend as their 1-substituted analogues **a**, **c**, and **d** (Figures S80–S81), indicating that the substitution position has little impact. For example, when the amine-1-substituted adamantanes **a**, **c**, or **d** were mixed with their corresponding 2-substituted analogues **a-2**, **c-2**, or **d-2** and analyzed by ^{1}H-NMR, both guests were encapsulated in nearly equal ratios (1.4:1 for **a**:**a-2**, 0.9:1 for **c**:**c-2**, and 1.2:1 for **d**:**d-2**, Figures 3 and S77–S79). These results indicate that the affinity is dictated not by the position of substitution (1- vs 2-), but by the nature of the substituent itself. This behavior is consistent with the pseudo-spherical shape of the adamantane core, which allows effective accommodation within the [8]CPP cavity regardless of substitution at a tertiary or secondary carbon.

The insight gained from these competitive studies prompted us to attempt the direct purification of a complex mixture containing **a**, **c**, **g**, **i**, and **l**. To this end, **4**·(BArF)$_8$ was combined with a chloroform solution of the mixed mono-adamantanes and excess [8]CPP. HRMS monitoring revealed that only **a** was encapsulated, while **c**, **g**, **i**, and **l** remained in solution (Figure S74). When only **c**, **g**, **i**, and **l** were present, encapsulation occurred exclusively for **c**, consistent with the competition studies (Figure S73). Hence, to design a practical purification protocol, we tested a solid-state encapsulation strategy. A small

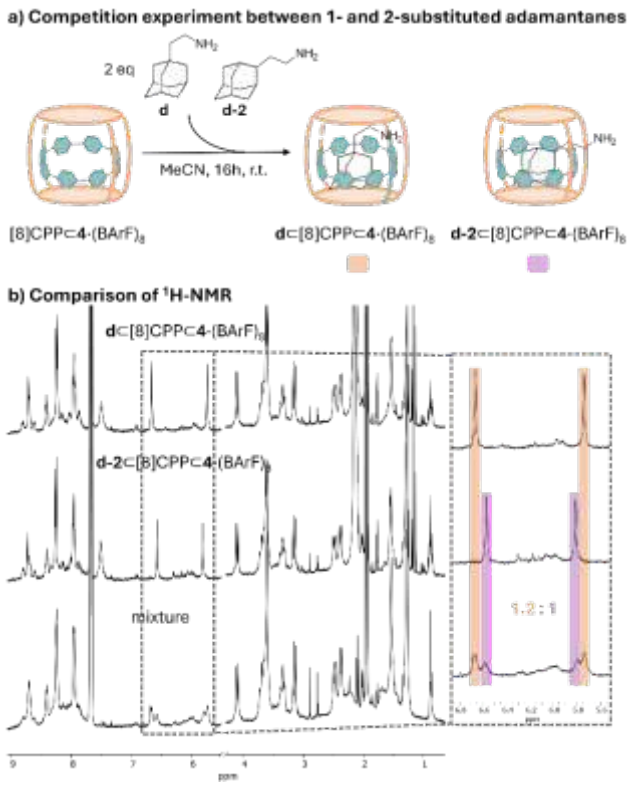

Figure 3. a) Competition experiment between 1- and 2-substituted adamantanes in the presence of [8]CPP⊂**4**·(BArF)$_8$. b) Stacked ^{1}H-NMR (CD_3CN) showing the formation of both Matryoshka complexes **d**⊂[8]CPP⊂**4**·(BArF)$_8$ (peaks of the [8]CPP marked in orange) and **d-2**⊂[8]CPP⊂**4**·(BArF)$_8$ (peaks of the [8]CPP marked in purple) in a 1.2:1 ratio.

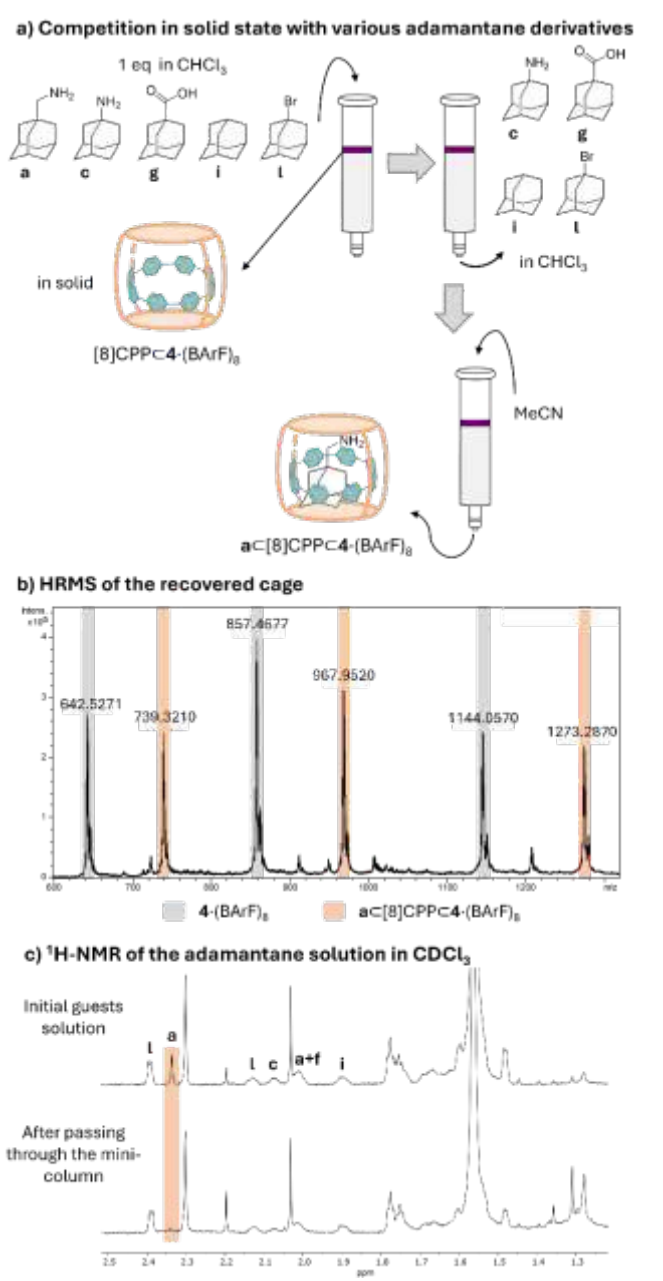

Figure 4. a) Schematic experiment showing the solid-state purification system used to purify **a** from a mixture of adamantane derivatives (**a**, **c**, **g**, **i**, and **l**, 1 eq of each). b) HRMS showing the formation and recovery of the single Matryoshka complex **a**⊂[8]CPP⊂**4**·(BArF)$_8$ (peaks marked in orange) and empty **4**·(BArF)$_8$ (peaks marked in grey). c) ^{1}H-NMR (in $CDCl_3$) of the initial solution of adamantane derivatives (top) and after passing it through the mini-column (bottom), observing the disappearance of a peak corresponding to guest **a**.

column packed with Celite® was loaded with solid [8]CPP⊂**4**·(BArF)$_8$, and a chloroform solution of **a**, **c**, **g**, **i**, and **l** was flashed through the column five times (Figure 4). This procedure efficiently trapped **a** in the Matryoshka assembly, whereas **c**, **g**, **i**, and **l** eluted in the chloroform fraction (Figures 4 and S75). The solid Matryoshka was subsequently rinsed with fresh chloroform and redissolved in MeCN. Subsequent acidic treatment disassembled the cage, releasing [8]CPP and **a**, which were readily recovered by flash chromatography. The efficient incorporation of guest **a** into [8]CPP⊂**4**·(BArF)$_8$ is attributed to the large cage entrances and the small size of the mono-adamantane. Notably, when empty **4**·(BArF)$_8$ was used in the solid state and flashed with a chloroform solution of [8]CPP and the mono-adamantane mixture, no encapsulation of either the nanoring or the mono-adamantanes was observed. This result indicates that the nanoring dimensions and the lack of dynamic gate breathing in the solid state prevent [8]CPP entry into the cage (Figure S76).

Affinity constants

Affinity constants between [8]CPP and the diamondoid guests were determined by ^{1}H-NMR titrations in $CDCl_3$, in which increasing amounts of the guest were added to a solution of fixed [8]CPP concentration (Figures S83–S87). Various adamantane derivatives were examined (**a**, **e**, **g**, **i**, **k**), revealing low association constants on the order of 2-60 M^{-1} (Table S1), indicating very weak host–guest interactions.

The affinity between **4**·(BArF)$_8$ and [8]CPP was also measured by ^{1}H-NMR titration in a CD_2Cl_2:CD_3CN (9:1) mixture to solubilize both components (Figure S88). A K_a value of (1.5 ± 0.11) × 10^3 M^{-1} was obtained (Table S1), which is two orders of magnitude lower than that reported for the analogous system with [10]CPP and the larger cage **6**·(BArF)$_8$.[27]

The affinity constant for the **a**⊂[8]CPP⊂**4**·(BArF)$_8$ complex was determined using a similar ^{1}H-NMR titration protocol (Figure S89). A solution containing both guests (**a** and [8]CPP) was added to a solution of empty **4**·(BArF)$_8$ at constant concentration in CD_2Cl_2:CD_3CN (9:1). A K_a value of (1.6 ± 0.6) × 10^5 M^{-1} was obtained (Table S1), representing an increase of two orders of magnitude from that of the [8]CPP alone. This result indicates that the presence of the adamantane derivative promotes encapsulation of [8]CPP, facilitating the formation of the Matryoshka complex.

Owing to the high K_a observed for the **a**⊂[8]CPP⊂**4**·(BArF)$_8$ Matryoshka assembly (>10^5 M^{-1}), we focused on its crystallization for single-crystal X-ray diffraction (SCXRD) analysis. Suitable crystals were obtained and measured at the SCXRD facility at the Alba-BCN synchrotron using carefully prepared capillaries containing mother liquor to prevent solvent loss and rapid amorphization. SCXRD analysis confirmed the formation of the expected metal-organic cage; however, the resolution within the internal cavity was limited, and only diffuse electron density was observed. This inner electron density is consistent in both shape and spatial distribution with the presence of the encapsulated [8]CPP, but it cannot be unambiguously assigned. To further support the proposed

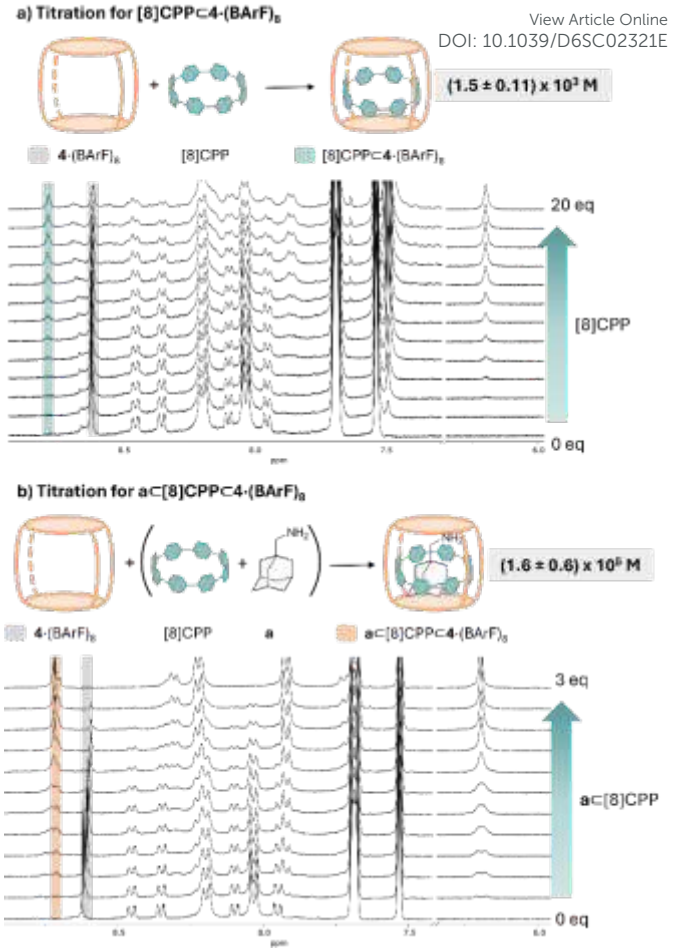

Figure 5. a) Titration experiment to extract the affinity constant for [8]CPP⊂**4**·(BArF)$_8$. Stacked ^{1}H-NMR (CD_2Cl_2) with the peaks of the empty cage marked in grey and peaks of [8]CPP⊂**4**·(BArF)$_8$ marked in blue. b) Titration experiment to extract the affinity constant for **a**⊂[8]CPP⊂**4**·(BArF)$_8$. Stacked ^{1}H-NMR (CD_2Cl_2) with the disappearing peaks of the empty cage marked in grey and appearing peaks of **a**⊂[8]CPP⊂**4**·(BArF)$_8$ marked in orange.

structural model, refinement attempts were made using a rigid fragment derived from quantum-chemical calculations. These attempts were unsuccessful due to the incompatibility between the crystallographic symmetry of the cage (P4) and the symmetry of the calculated guest. Even after reducing the symmetry during refinement, a satisfactory fit for the fully encapsulated molecule could not be obtained. Nevertheless, partial refinement of the encapsulated nanoring was achieved, allowing the localization of four benzene rings of the [8]CPP within the cavity (Figure S99) and thereby confirming the encapsulation of [8]CPP inside cage **4**.

Computational studies

Since SCXRD characterization was inconclusive, molecular dynamics (MD) simulations were carried out to gain further insight into the positioning of mono-adamantane⊂[8]CPP complexes within the cage cavity. In all cases, the mono-adamantane guest together with [8]CPP was manually placed

View Article Online
DOI: 10.1039/D5SC03315E

inside **4**·Cl_8 as the starting configuration for the simulations. Simulations were performed with explicit MeCN as solvent and Cl^- ions as a model counteranion for $BArF^-$. Simulations of [8]CPP alone inside **4**·Cl_8 revealed that the encapsulated nanoring remains dynamic and is not well-centered within the cage cavity, instead shifting toward one of the cage windows (Figure S91). This behavior is likely driven by the maximization of π–π interactions between the phenyl rings of [8]CPP and the cage clips, as evidenced by the noncovalent interaction (NCI) surface analysis (Figure S94). For the Matryoshka **a**⊂[8]CPP⊂**4**·Cl_8, the complex adopts a well-defined orientation, with [8]CPP again displaced toward a cage window (Figures 6a and S91). Notably, the amine moiety of **a** forms effective apical coordination to the Zn–porphyrin, while π–π interactions between [8]CPP and the clips are maintained. This translates into a highly stable complex, as further illustrated by the NCI surface analysis (Figures 6a and S94). These results indicate that the CH_2 spacer between the adamantane core and the amine group is essential for enabling effective N···Zn coordination while minimizing steric clash between the porphyrin and [8]CPP. Additionally, the NH_2 group interacts with [8]CPP, stabilizing the nanoring in a fixed orientation (Figure S95b).

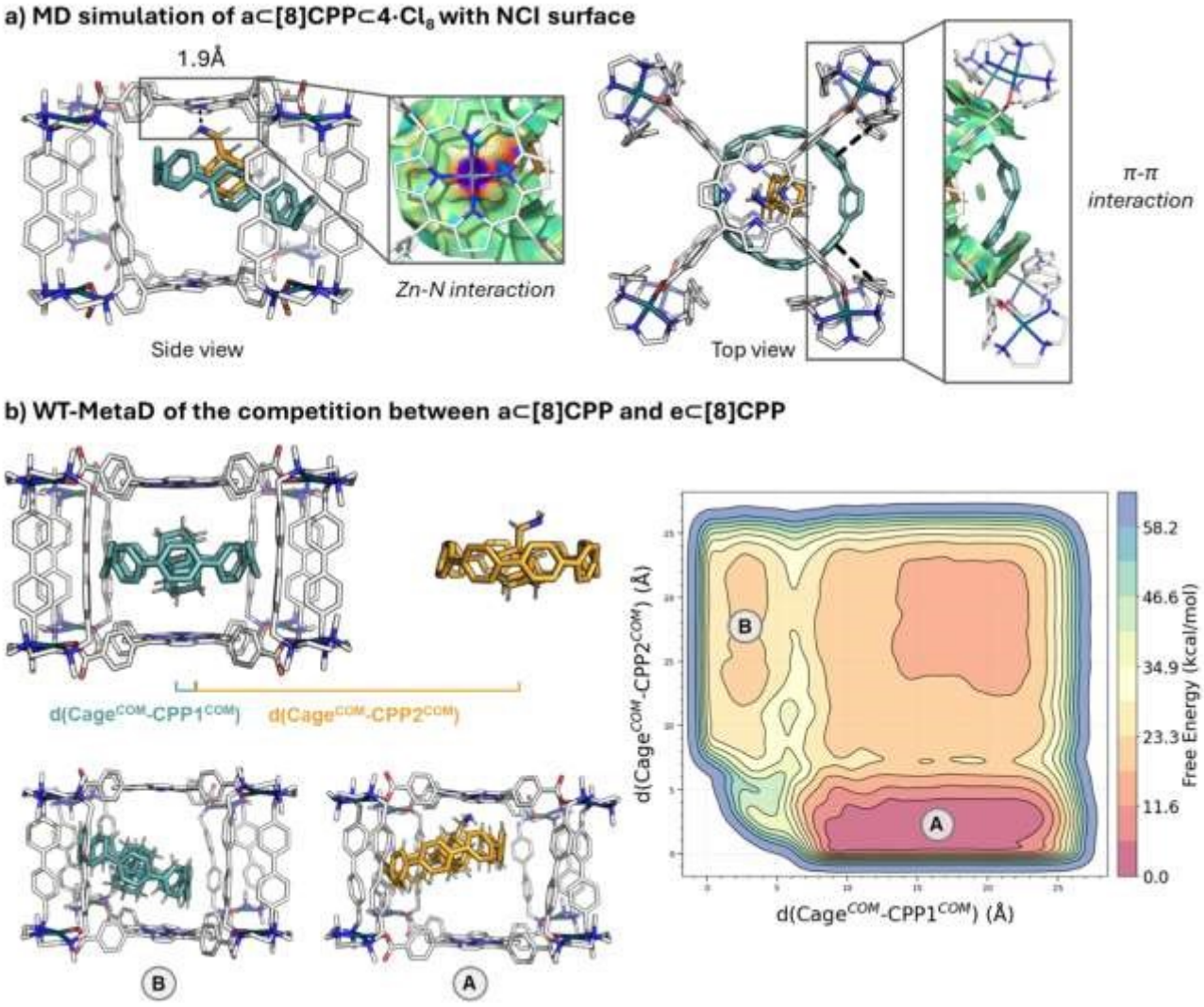

Figure 6. a) Snapshot of the MD simulations of **a**⊂[8]CPP⊂**4**·Cl_8 with side and top views. Zn···N interaction between the porphyrin and the amine group of the adamantane is shown in a black dashed line with a distance of 1.9 Å, with the representation of the NCI surface (weak van der Waals interactions in green and positive interactions in blue). π-π interactions between [8]CPP and the phenyl rings on the clips are also represented with a black dashed line, with the representation of the NCI surface. Hydrogens of the cage and the [8]CPP have been omitted for clarity. b) Description of the two CVs used in the WT-MetaD simulations for the competition between **a**⊂[8]CPP and **e**⊂[8]CPP, being the distance between the center of masses of the cage ($Cage^{COM}$) and the center of masses of each CPP ($CPP1^{COM}$ for the diamantane **e** in green and $CPP2^{COM}$ for the adamantane **a** in orange). Free energy landscape for the competition, with the two metastable states (A and B) corresponding to the encapsulation of each complex.

View Article Online
DOI: 10.1039/D6SC02321E

ARTICLE

In the case of **b**⊂[8]CPP⊂**4**·Cl_8, the presence of the α-methyl substituent prevents full encapsulation of the adamantane core within [8]CPP (Figure S95a), and no NH_2···[8]CPP interaction is observed due to the increased distance (Figure S95b), resulting in reduced stabilization and lower binding affinity. For **c**⊂[8]CPP⊂**4**·Cl_8, the [8]CPP displays increased dynamic mobility, rotating between cage windows. Here, the amine is directly attached to the adamantane core, and full encapsulation by [8]CPP is hindered due to steric clash with the Zn–porphyrin unit (Figure S95b), leading to a less stable complex with reduced affinity. By contrast, **d**⊂[8]CPP⊂**4**·Cl_8, which features a longer –$CH_2CH_2NH_2$ linker, exhibits effective Zn···N coordination along with π–π interactions between [8]CPP and the cage clips. Guests **e-g**, lacking the N···ZnTCPP anchoring motif, behave similarly, with [8]CPP preferentially positioned toward a single window. For diamantane **e**, the guest adopts a vertical orientation relative to the porphyrin planes and is encapsulated by [8]CPP along its shortest axis (Figure S93).

NCI calculations of a representative frame for the **e**⊂[8]CPP⊂**4**·Cl_8 and **i**⊂[8]CPP⊂**4**·Cl_8 complexes show that the diamantane **e** presents more interactions with the [8]CPP than adamantane **i** (NCI volume of 737.31 $Å^3$ for **e** and 586.86 $Å^3$ for **i**), in line with experimental observations (Figure S98). For **f** and **g**, Zn···O interactions are observed (Figure S91). Finally, in **h**⊂[8]CPP⊂**4**·Cl_8, the smallest amine-containing adamantane, increased guest mobility is observed due to its small size, which precludes effective Zn–TCPP interaction while maintaining favorable interactions with [8]CPP. This behavior aligns with its weak binding affinity, being the last of the preferred guests in the series (Figure 2a). MD simulations of the 2-substituted adamantanes (**a-2**, **c-2**, and **d-2**) revealed similar trends to their corresponding 1-substituted analogues (Figure S92).

To gain further insight into the competition experiments, well-tempered metadynamics (WT-MetaD) simulations were performed to model the exchange between two adamantane⊂[8]CPP complexes of differing affinity. Adamantanes **a** and **e** were selected due to the markedly different affinities. In the WT-MetaD setup, the **e**⊂[8]CPP complex was initially placed inside the cage **4**·Cl_8, while **a**⊂[8]CPP was positioned outside. Four 1 μs replicas were conducted, using two collective variables (CVs) corresponding to the distances between the center of mass of the cage and each [8]CPP (see Figure 6b and SI for details). The simulations first revealed rapid release of **e**⊂[8]CPP and simultaneous encapsulation of **a**⊂[8]CPP (Figures 6b and S96–S97). Subsequently, multiple binding and unbinding events involving both guest⊂[8]CPP complexes were observed throughout the simulations. Overall, **a**⊂[8]CPP remained encapsulated for longer periods, reflecting its higher affinity imparted by the N···ZnTCPP anchoring handle, whereas **e**⊂[8]CPP spent a larger fraction of time unbound. These results confirm the relative experimentally observed affinity trend and underscore the critical role of the anchoring interaction in governing guest selectivity.

Conclusions

We have designed a three-shell Matryoshka assembly platform that enables the cooperative encapsulation of diamondoids and nanorings within the cavity of a tetragonal prismatic supramolecular cage. Selective encapsulation is achieved by fine-tuning the substitution pattern of mono-adamantane derivatives, which modulates a dual stabilization mechanism that combines confinement within the [8]CPP nanoring and apical Zn-TCPP anchoring interactions. This Matryoshka assembly operates through an all-in-one strategy: encapsulation is inefficient for [8]CPP or diamondoids individually and becomes highly efficient when all three components act cooperatively. As a result, the Matryoshka architecture allows the selective purification of diamondoid mixtures both in solution and, remarkably, in the solid state via a simple filtration–redissolution protocol. This level of selectivity among complex diamondoid mixtures surpasses that achievable by chromatographic techniques. We anticipate that this approach will inspire new supramolecular strategies for the purification of adamantane-based pharmaceuticals and higher diamondoids of relevance to nanotechnological applications.

Author contributions

C. S. performed the experiments and MD studies. T. P. contributed with experiments on multishell assemblies using cage **4**·$(BArF)_8$. I. I. and D. M. performed the XRD studies. F.F. and X. R. supervised and conceptually design the study, discussed the results, and wrote the manuscript.

Conflicts of interest

There are no conflicts to declare.

Data availability

The data that support the findings of this study are available within the article and supplementary information (SI). Supplementary information is available, including materials, instrumentation, experimental procedures, spectroscopic and photophysical characterization of all compounds, and

computational details. Computational data is available via Zenodo under the following link: https://doi.org/10.5281/zenodo.18378892

Acknowledgements

We thank MCIN Spain (PID2022-136970NB-I00 and TED2021-130573B-I00 to X.R, RYC2020-029552-I, and PID2022-141676NB-I00 to F.F.) and Generalitat de Catalunya (2021SGR00475, 2021SGR00487). C.S. and T.P thank UdG and MCIN for IF and FPU PhD grants, respectively. X.R thanks an ICREA-Academia award. I.I. and D.M. acknowledge the Catalan AGAUR (project 2021 SGR 00458), and the CERCA program/Generalitat de Catalunya. We thank Judith Juanhuix for support in the BL13-XALOC. We also thank the Ochoa Centers of Excellence program, Grant CEX2021-001214-S, funded by MCIN/AEI/10.13039.501100011033 to D.M.

Notes and references

1. W. L. Davies, R. R. Grunert, R. F. Haff, J. W. McGahen, E. M. Neumayer, M. Paulshock, J. C. Watts, T. R. Wood, E. C. Hermann and C. E. Hoffmann, *Science*, 1964, **144**, 862-863.
2. L. Wanka, K. Iqbal and P. R. Schreiner, *Chem. Rev.*, 2013, **113**, 3516-3604.
3. V. M. Dembitsky, T. A. Gloriozova and V. V. Poroikov, *Biochem. Biophys. Res. Commun.*, 2020, **529**, 1225-1241.
4. E. T. Warda, M. B. El-Ashmawy, E.-S. E. Habib, M. S. M. Abdelbaky, S. Garcia-Granda, S. Thamotharan and A. A. El-Emam, *Sci. Rep.*, 2022, **12**, 21058.
5. A. S. Monto, S. E. Ohmit, K. Hornbuckle and C. L. Pearce, *Antimicrob. Agents Chemother.*, 1995, **39**, 2224-2228.
6. M. Bonsir, A. R. Kennedy and Y. Geerts, *ChemistryOpen*, 2022, **11**, e202200031.
7. K.-W. Yeung, Y. Dong, L. Chen, C.-Y. Tang, W.-C. Law and G. C.-P. Tsui, *Nanotechnol. Rev.*, 2020, **9**, 650-669.
8. W. A. Clay, Z. Liu, W. Yang, J. D. Fabbri, J. E. Dahl, R. M. K. Carlson, Y. Sun, P. R. Schreiner, A. A. Fokin, B. A. Tkachenko, N. A. Fokina, P. A. Pianetta, N. Melosh and Z.-X. Shen, *Nano Lett.*, 2009, **9**, 57-61.
9. T. Kusaba, Y. Kuranaga and S. Miyamoto, *J. Chem. Eng. Jpn.*, 2013, **46**, 262-270.
10. Y. Yao, C. Shao, S. Wang, Q. Gong, J. Liu, H. Jiang and Y. Wang, *Commun. Chem.*, 2024, **7**, 43.
11. L.-J. Wang, Z.-E. Zhang, Y.-Z. Zhang and Y.-F. Han, *Angew. Chem. Int. Ed.*, 2024, **63**, e202407278.
12. M. Yao, P. Stenmark, E. Abou-Hamad, F. Nitze, J. Qin, C. Goze-Bac and T. Wågberg, *Carbon*, 2011, **49**, 1159-1166.
13. Y. Li, Z. Yao, B.-B. Liu, L. Wang, C. Pei, Y. Yuan and J. Ai, *Philos. Mag.*, 2019, **99**, 401-418.
14. K. Iizuka, H. Takezawa and M. Fujita, *Angew. Chem. Int. Ed.*, 2025, **64**, e202422143.
15. R. Jasti, J. Bhattacharjee, J. B. Neaton and C. R. Bertozzi, *J. Am. Chem. Soc.*, 2008, **130**, 17646-17647.
16. J. Xia, J. W. Bacon and R. Jasti, *Chem. Sci.*, 2012, **3**, 3018-3021.
17. D. Lu, Q. Huang, S. Wang, J. Wang, P. Huang and P. Du, *Front. Chem.*, 2019, **7**.
18. Y. Xu and M. von Delius, *Angew. Chem. Int. Ed.*, 2020, **59**, 559-573.
19. T. Iwamoto, Y. Watanabe, T. Sadahiro, T. Haino and S. Yamago, *Angew. Chem. Int. Ed.*, 2011, **50**, 8342-8344.
20. X. Chang, Y. Xu and M. von Delius, *Chem. Soc. Rev.*, 2024, **53**, 47-83.
21. F. M. Steudel, E. Ubasart, L. Leanza, M. Pujals, T. Parella, G. M. Pavan, X. Ribas and M. von Delius, *Angew. Chem. Int. Ed.*, 2023, **62**, e202309393.
22. F. M. Steudel, C. Sabrià, M. D. Piane, F. Feixas, X. Ribas, G. M. Pavan and M. von Delius, *Chem. Sci.*, 2025, **16**, 21908-21916.
23. H. Kwon, B. S. Newell and C. J. Bruns, *Nanoscale*, 2022, **14**, 14276-14285.
24. H. Kwon and C. J. Bruns, *Nano Research*, 2022, **15**, 5545-5555.
25. C. García-Simón, M. Garcia-Borràs, L. Gómez, T. Parella, S. Osuna, J. Juanhuix, I. Imaz, D. Maspoch, M. Costas and X. Ribas, *Nat. Commun.*, 2014, **5**, 5557.
26. E. Ubasart, C. García-Simón, M. Pujals, K. Asad, N. Chronakis, T. Parella and X. Ribas, *Org. Chem. Front.*, 2021, **8**, 4101-4105.
27. E. Ubasart, O. Borodin, C. Fuertes-Espinosa, Y. Xu, C. García-Simón, L. Gómez, J. Juanhuix, F. Gándara, I. Imaz, D. Maspoch, M. von Delius and X. Ribas, *Nat. Chem.*, 2021, **13**, 420-427.
28. C. Fuertes-Espinosa, C. García-Simón, M. Pujals, M. Garcia-Borràs, L. Gómez, T. Parella, J. Juanhuix, I. Imaz, D. Maspoch, M. Costas and X. Ribas, *Chem*, 2020, **6**, 169-186.
29. C. García-Simón, C. Colomban, Y. A. Çetin, A. Gimeno, M. Pujals, E. Ubasart, C. Fuertes-Espinosa, K. Asad, N. Chronakis, M. Costas, J. Jiménez-Barbero, F. Feixas and X. Ribas, *J. Am. Chem. Soc.*, 2020, **142**, 16051-16063.
30. C. García-Simón, R. Gramage-Doria, S. Raoufmoghaddam, T. Parella, M. Costas, X. Ribas and J. N. H. Reek, *J. Am. Chem. Soc.*, 2015, **137**, 2680-2687.

View Article Online
DOI: 10.1039/D6SC02321E

Data availability

The data that support the findings of this study are available within the article and supplementary information (SI). Supplementary information is available, including materials, instrumentation, experimental procedures, spectroscopic and photophysical characterization of all compounds, and computational details. Computational data is available via Zenodo under the following link: https://doi.org/10.5281/zenodo.18378892